

Standing Tall: Robust Fall Prediction for Bipedal Robots

Gokul Prabhakaran, Jessy W. Grizzle, and M. Eva Mungai

Abstract—This paper extends the fall prediction algorithm from [1] to a real-time/online setting, implemented in both hardware and simulation. This yields results comparable to the offline version, maintaining a zero false positive rate, sufficient lead time, and accurate lead time prediction. Additionally, it achieves a high recovery rate. The paper also evaluates the fall prediction algorithm against omnidirectional faults and introduces an improved algorithm capable of reliably predicting falls and lead times across a wider range of faults in full-sized robots. Compared to [1], the proposed algorithm performs significantly better across all metrics, such as false positive rate, lead time, accuracy, and response time, demonstrating the algorithm’s efficacy for real-time fall prediction in bipedal robots.

I. INTRODUCTION

Humanoid robots have attracted significant attention over the past year, with a surge in companies developing general-purpose humanoids for both home and factory applications. Although some humanoids have already been deployed in home and factory environments, their widespread adaptation, especially in unstructured or unknown environments, remains limited [2]–[11]. A key challenge in broadly deploying humanoid robots in these environments is their high-dimensional, hybrid nature, which, paired with their smaller support polygons, makes it particularly difficult to maintain stable motion, especially in unstructured terrains in the presence of disturbances and uncertainties. While a well-designed controller can mitigate the effects of disturbances and uncertainties, the unpredictable nature of real-world operations makes falls inevitable. As a result, it is imperative to implement fall prediction algorithms alongside robust controllers, especially in real-time operations. Therefore, this paper extends the previously proposed fall prediction framework [1] to real-time operations, analyzes the algorithm’s robustness to omnidirectional disturbances during the task of standing, and offers pathways to expand its capabilities. Note that the task of standing was chosen in [1] as a precursor to scaling up to more dynamic motions.

A. Background

The overarching objective of a fall prediction algorithm is to accurately predict falls with sufficient time to implement a recovery strategy. As discussed in [1] and [12], faults can be a precursor to a bipedal robot falling. Faults are defined as unforeseen deviations in one or more operational variables. Based on their temporal behavior, they can be categorized as either **abrupt**, **incipient**, or **intermittent**. Abrupt faults are sudden, incipient faults develop gradually, and intermittent

faults occur sporadically. Intermittent faults are comprised of abrupt and incipient faults [13]. In this paper, we refer to faults that lead to a fall as **critical faults**. The term **lead time** is used to describe the difference in time between the prediction of a fall and its actual occurrence, while **response time** is the difference in time between when a critical fault is introduced and when a fall is predicted. A trajectory or state is considered **unsafe** if it leads to a fall, and **safe** if it does not.

B. Literature Review

While there are numerous fall prediction algorithms for bipedal robots, ranging from static threshold-based methods to machine learning approaches [14], [15], the implementation of algorithms capable of real-time/online prediction of falls caused by abrupt, incipient and intermittent faults in full-sized humanoids, in hardware, remains limited.

For clarity, in addition to the detection of the three types of faults and the size of the robot, we also distinguish between four experimental settings: offline with simulation data, offline with hardware data, online in simulation, and online in hardware.

The fall prediction algorithm proposed in [16] uses sensor fusion to predict falls in real-time, across various terrains and during dynamic motions such as squatting, in simulation and hardware for the 1.92m WALK-MAN humanoid [17]. However, the analysis is limited to falls caused by abrupt faults. Similarly, the SVM-based algorithm from [18] is tested online in hardware and simulation for the 1.6m BHR-6 robot during walking and standing tasks, and only considers abrupt faults.

In contrast, while [19], [20], [21], and [22] do not explicitly address all three faults, their analyses are based on scenarios that may encompass all temporal fault categories—for instance, varying the robot’s initial state [19], robot-to-robot interactions [20], walking on uneven terrain [21], and motor failures [22]. Despite the potential inclusion of all three faults, the analyses in [19] and [21] are limited to offline simulations of the 1.43m planar bipedal robot Rabbit [23] and the 90cm NUGUS humanoid robot, respectively. While [22] uses both hardware and simulation data to evaluate their algorithm on the 1.82m Q1 humanoid robot and a Cassie bipedal robot—originally 1m tall [24]—fitted with a torso, their analysis does not include online hardware experiments. On the other hand, [20] conducts their analysis online in both hardware and simulation, though it is limited to the 0.57m tall Nao H25 robot [25], [26].

In comparison to the other approaches, building on previous work in [12], [1] develops a 1D CNN model capable of

{Robotics, Robotics, Robotics} Department, University of Michigan, Ann Arbor, MI, USA. {gok, grizzle, mungai}@umich.edu

predicting falls from all three faults and estimating lead times for the 1.6m tall bipedal robot Digit [27], both in simulation and hardware. The algorithm was validated on a new open-source dataset for the Digit platform [28]. However, the study is limited to offline prediction in a planar standing task, where faults are simulated by applying forces to the robot’s back center. Despite this limitation, the model demonstrates high prediction accuracy in offline settings.

C. Objective

Therefore, the objective of this paper is to extend [1]’s algorithm, which we term the **nominal** algorithm, to an online setting, both in hardware and simulation, and to improve the algorithm’s performance to omnidirectional faults during the task of standing, while adhering to the requirements outlined in [1]. Specifically, this paper aims to:

- Maintain the nominal algorithm’s goal of reliably detecting imminent falls caused by abrupt, incipient, and intermittent faults, with sufficient lead time for a full-sized bipedal robot, while also accurately predicting the lead time.
- Implement the nominal fall prediction algorithm online, both in hardware and in simulation.
- Evaluate the performance of the nominal algorithm on critical faults applied in the sagittal and frontal plane at various angles and locations on the robot, using the same metrics as [1]: false positive rates, lead time, and response time.
- Propose a method for robustifying the nominal algorithm against a broader set of faults.

As in [1], the robot is considered to have fallen if its center of mass is less than 10 percent of its initial height, and the minimum desired lead time is set to 0.2 seconds.

Achieving the objective outlined above is challenging due to several factors: the masking effects of the controller, the sporadic nature of intermittent faults, the trade-off between lead time and false positive rates, and the crowding effect of incipient faults [29]. Furthermore, the decreasing number of available data points as the lead time increases [1], along with the diverse range of faults, complicates the prediction of falls. Implementing the algorithm online introduces additional challenges, including the need for fast inference times and the management of communication delays between different components of the fall prediction algorithm and other processes, such as the controller.

D. Contributions

The main contributions of this paper are as follows:

- Implementation of the nominal fall prediction algorithm online, both in hardware and simulation
- Extension of the open-source dataset [28] to include critical and non-critical faults, introduced by applying angled and non-angled forces at various locations in the sagittal and frontal planes of the robot
- Analysis of the nominal fall prediction algorithm against a broader range of faults.

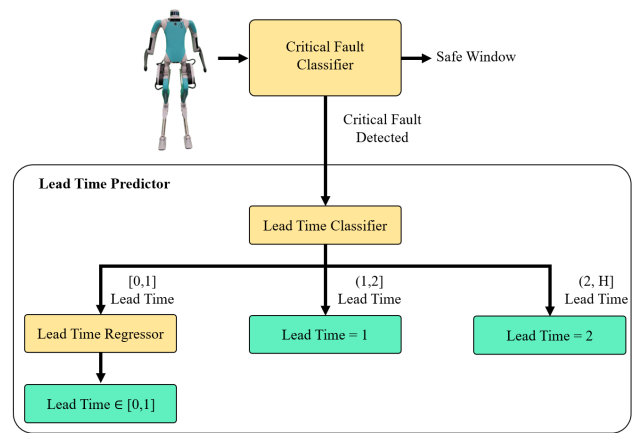


Fig. 1: The fall prediction algorithm proposed in [1] is comprised of three components: a critical fault classifier, a lead time classifier, and a lead time regressor. The green boxes depict the algorithm’s predicted lead time.

- Introduction of a fall prediction algorithm capable of predicting falls caused by a wider range of critical faults while also predicting lead time.

II. SYSTEM OVERVIEW: NOMINAL FALL PREDICTION ALGORITHM, HARDWARE DESCRIPTION, AND EXPERIMENTAL SETUP

This section provides a brief overview of the fall prediction algorithm introduced in [1], along with a concise summary of the hardware and experimental setup used in this paper, which are similar to [1].

A. Fall Prediction Algorithm Framework

The 1D CNN-based fall prediction algorithm introduced in [1] consists of three parts: a critical fault classifier, a lead time classifier, and a lead time regressor. The critical fault classifier identifies critical faults, while the lead time classifier and the regressor work together to predict the lead time. The lead time classifier divides the lead time into three intervals: $[0, 1]$, $(1, 2]$, and $(2, H]$. If the lead time is classified into the $[0, 1]$ interval, the lead time regressor calculates the lead time. Otherwise, the lead time is considered as the infimum of the interval. To prioritize the most recent data points, sliding windows with 10 data points are used. The algorithm is trained with trajectories sampled at approximately 40 Hz. Figure 1 depicts the algorithm’s framework.

B. Hardware Description

We utilize the bipedal robot Digit [27] developed by Agility Robotics. Digit is approximately 1.6m, weighs 48 kg and has 30 degrees of freedom, 20 actuated joints, and an integrated perception system. Figure 2 illustrates Digit’s kinematic architecture.

C. Experimental Setup

1) *Simulation:* We employ the use of Agility’s MuJoCo-based simulator with a standing controller designed to maintain the center of mass and zero moment point inside the

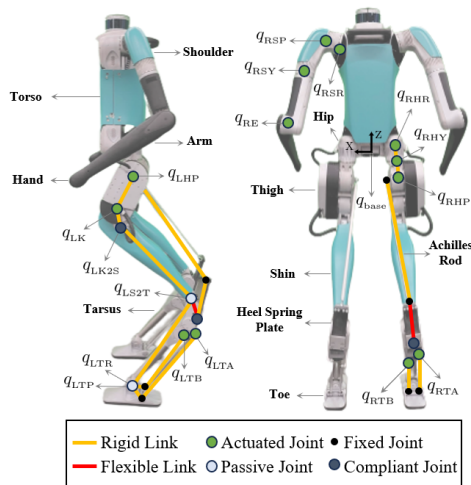


Fig. 2: Kinematics architecture of the Digit robot by Agility Robotics [1], [27].

support polygon [30]. This controller will be referred to as the **nominal controller**. The nominal controller can stabilize incipient faults up to a force of 28.8N and abrupt faults up to 207.4N [1]. Abrupt and incipient faults are emulated in simulation by applying impulsive and trapezoidal pushing forces, respectively, to the back center of the robot, denoted as region F in Figure 5. To introduce slight oscillations to the robot’s standing posture, random abrupt forces within the range of 0 - 202.4N are introduced, but only the windows during and after the fault introduction are passed to the fall prediction algorithm.

2) *Hardware*: In contrast to the simulation setup, where faults are applied to Digit’s back center, this location was avoided during hardware experiments as it houses the on-board computer and is vulnerable to damage. Instead, faults are introduced in region C on the back of the torso, as shown in Figure 5, by applying pushing forces with a pole. To capture the gradual nature of incipient faults, the pole is first positioned on the robot before applying force. To prevent potential damage during experiments, the robot is secured to a gantry using a slack cable, and motor power is disabled upon detecting a fall.

III. ONLINE FALL PREDICTION

This section assesses the performance of the nominal fall prediction algorithm when executed online in both simulation and hardware.

A. Experimental Setup

In the hardware setup, we do not have direct access to the main computer, so we interact with the robot by sending commands and receiving state information over UDP at approximately 1 kHz. This information is processed by the nominal controller, which publishes topics via ROS also at roughly 1 kHz. The robot is connected to an Alienware m15 computer with an Intel i9-12900H processor via Ethernet. This computer runs both the fall prediction algorithm and

the nominal controller. The simulation emulates this asynchronous setup. However, it is run on a machine with an Intel i9-7900x processor.

To run the fall prediction algorithm online, the robot is first initialized in a standing position with the nominal controller. The robot’s state and the torques commanded by the nominal controller are then queried via ROS [31] at a rate of 400Hz. The fall prediction algorithm, however, runs at 40 Hz. Therefore, features for the algorithm are computed using newly queried data every 40 Hz. Once enough features are available to form a window, model inference is performed continuously until a fall is predicted. Once a fall is predicted, the recovery controller, if one is available, is activated. Note 40 Hz is chosen to match the sampling frequency of the trajectories in [1].

Building on the offline analysis presented in [1], the algorithm’s performance is evaluated using lead time, false positive rate, and response time. In addition to these metrics, we introduce a new metric to assess the algorithm’s effectiveness: the **recovery rate**. The recovery rate measures the number of unsafe trajectories that are stabilized by switching to a recovery controller when a critical fault is detected. We report the recovery rate only for simulation tests due to the difficulty of replicating the same fault multiple times in hardware. Since implementing a recovery controller falls outside the scope of this work, we utilize Agility’s base controller, which already incorporates a fall prevention strategy.

As in the offline tests, faults are emulated by applying horizontal forces of varying magnitudes to regions C and F in Figure 5 for hardware and simulation, respectively. The online evaluations are also limited to abrupt and incipient faults, as the algorithm’s effectiveness in detecting intermittent faults, as demonstrated in [1], depends on accurately identifying critical abrupt and incipient faults.

B. Simulation Results

To assess the fall prediction algorithm’s performance online in simulation and compare it to the offline results presented in [1], we replicate the 200 abrupt and incipient tests used in the offline evaluation and apply the algorithm to these tests as described in Section III-A. The average runtime of the fall prediction algorithm is approximately 0.0045s, with the total inference time of the 1D CNN models being 0.004s and the computation of the features taking 0.0005s.

As shown in Table I, the true average lead time for the online execution is 0.01s higher than the offline execution. This minor discrepancy in fault detection is primarily due to communication delays, which cause the online algorithm to occasionally run slower, averaging 40 Hz but sometimes dipping to lower rates. As a result, windows with features are sampled at intervals slightly greater or less than 40 Hz, leading to differences in the timing of fault detection. These timing variations also contribute to small changes in the average response time and predicted lead time, which decrease by 0.02s and increase by 0.04s, respectively, compared to the offline results. The difference between the average

true lead time and predicted lead time is 0.03s for the online execution and 0.02s for the offline execution. Both the online and offline evaluations report an average false positive rate of 0. Given the small differences between the online and offline results, we can conclude that the algorithm’s online performance is closely aligned with the offline results. Furthermore, the 0.97 recovery rate for the unsafe trajectories demonstrates the effectiveness of running the fall prediction algorithm online. Figure 3 showcases the results of switching vs not switching to a recovery controller when the nominal fall prediction algorithm detects a critical fault.

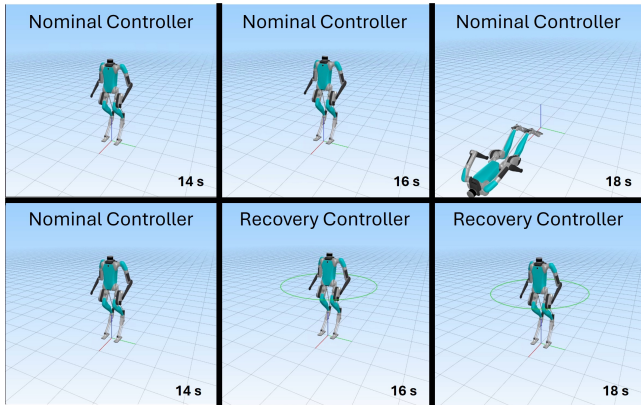


Fig. 3: Showcases the results of switching vs not switching to a recovery controller when the nominal fall prediction algorithm correctly detects a critical abrupt fault. The fault is introduced at 15s.

TABLE I: Online vs Offline Average Simulation Results of the Fall Prediction Algorithm Evaluated on Abrupt and Incipient Faults

Operation	Predicted Lead Time	True Lead Time	False Positive Rate	Response Time (s)	Recovery Rate
Offline	1.18	1.16	0.0	0.44	N/A
Online	1.14	1.17	0.0	0.42	0.97

C. Hardware Results

Given that [1] demonstrates the effectiveness of the fall prediction algorithm in detecting critical faults offline in both hardware and simulation, and as shown in the previous section, the algorithm’s offline performance is indicative of its online performance in simulation, we now seek to evaluate the algorithm’s inference time in hardware. To accomplish this, we execute the algorithm online in hardware 13 times, emulating 8 abrupt faults and 6 incipient faults in a manner similar to the setup described in [1]. Due to the challenges of replicating the same fault twice in hardware and to prevent potential damage to the robot, all tests are conducted with the recovery controller in the loop.

Out of the 8 abrupt faults, 4 are detected as critical faults, and 3 of the 6 incipient faults are identified as critical faults. The average predicted lead time of the entire algorithm

is 1.04s. This is the same as the offline hardware results reported in [1] and 0.1s lower than the results obtained in the online simulation. This deviation can be attributed to the smaller number of hardware online tests, which do not encompass as broad a range of critical faults. Note that we only report the average predicted lead time, as measuring the force application time and hence the response time online without force sensors proved challenging. Additionally, false-positive rates are unknown since the recovery controller is triggered whenever falls are detected.

The average runtime of the fall prediction algorithm for the hardware setup is 0.0061s, which is comparable to the algorithm’s runtime in simulation. The 0.0016s difference in runtime is negligible, given the algorithm’s sampling rate of 0.025s (40Hz). Furthermore, the nominal controller publishes at about 1kHz in both hardware and simulation. The negligible difference in runtime for the fall prediction algorithm between simulation and hardware, the small sim-to-real gap demonstrated offline in [1], and the similarity in performance when executed offline and online in simulation, as shown in Table I, suggest that the algorithm’s performance in simulation reliably translates to hardware, further validating its real-world applicability. Figure 4 demonstrates the fall prediction algorithm detecting a critical fault online in hardware.



Fig. 4: The nominal fall prediction algorithm detects a critical incipient fault and switches to the recovery algorithm

IV. ANALYSIS OF FALL PREDICTION FRAMEWORK PERFORMANCE

Given that the fall prediction algorithm was trained on abrupt and incipient faults introduced by applying pushing forces to region F at the torso back, as shown in Figure 5, and with features defined exclusively within the sagittal plane, it is not expected to perform well on faults outside its training distribution, such as those introduced by pushing the robot on its sides [32]. However, since the robot training data also included several trajectories where the robot rocked before falling on its front or back along the sagittal plane, it raises the question of whether the algorithm can handle faults introduced by applying forces at different locations and angles, such as the front of the torso. To address this, we evaluate the performance of the three components of the fall prediction algorithm across a broad range of faults. We limit our analysis here to abrupt and incipient faults for reasons similar

to those discussed in Section III. Additionally, the evaluation is conducted offline. However, given the negligible difference in performance between online and offline execution, as presented in Section III, we can reasonably conclude that the offline results presented here are indicative of the algorithm’s performance in real-time, online scenarios. Furthermore, the results in [1] suggest that the performance of the individual components directly translates to the overall performance of the algorithm. Note that the Digit open-source dataset, [28], will be extended to include the trajectories used here.

A. Data Generation

To assess the algorithm’s robustness across a wider range of faults, abrupt and incipient faults are emulated using pushing forces as described in [1]. The test dataset is generated by applying both angled and non-angled forces at 16 distinct locations on the robot, distributed across the sagittal and frontal planes. These locations are grouped into four regions: torso back, torso front, right side, and left side, with five points on the back, five on the front, and three on each side. Figure 5 illustrates the regions and points where the forces are applied.

For each of the 16 locations, 100 trajectories are generated for both abrupt and incipient faults, resulting in 200 trajectories per location, using both angled and non-angled pushes. For convenience, we term critical faults that are introduced by angled and non-angled forces as critical angled and non-angled faults, respectively. Angled forces are applied by selecting the magnitudes of the x and y components of the force, as well as the angle of the force relative to the transverse plane of the robot. The x -component magnitude is chosen such that applying a non-angled x force causes a fall in approximately half of the trajectories (for both the torso back and front). Similarly, the y -component magnitude is set to produce a fall in about half of the trajectories when non-angled y forces are applied (for the torso sides). The angle of the force relative to the transverse plane is randomly selected from a uniform distribution within the range of $[-45^\circ, 45^\circ]$. These angles were determined through empirical testing, where the physical robot was pushed at various angles to identify the range within which it could be effectively disturbed. Similar to [1], to ensure slight oscillations are present in the robot’s standing posture, random impulsive forces are introduced, but only windows during and after the fault introduction are used for fall prediction.

B. Nominal Critical Fault Classifier Results

In [1], the critical fault classifier demonstrated impressive results by detecting abrupt and incipient faults, achieving an average lead time of 1.52 seconds, an average response time of 0.44 seconds, and an average false positive rate of 0 when evaluated on unsafe trajectories derived in a similar manner to its training set. We refer to these results as **in-distribution results**.

When assessed on a broader range of abrupt and incipient critical faults, as described in the previous section, the classifier achieves an average response time comparable to the

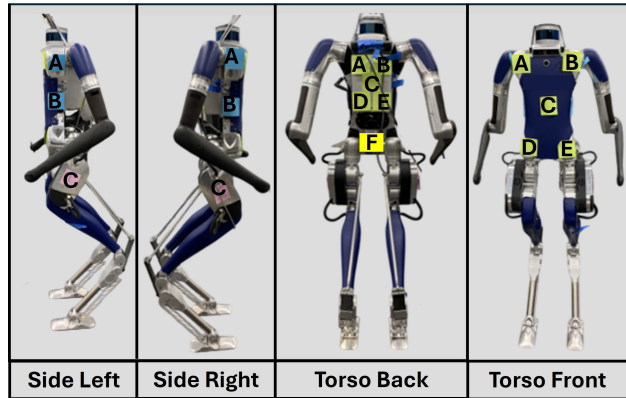


Fig. 5: Stickers in 16 positions indicating where faults were introduced. This includes (leftmost) 3 positions on the left side, (2nd from left) 3 positions on the right, (2nd from the right) 5 positions on the back of the torso, and (rightmost) 5 positions on the front of the torso.

in-distribution results, as shown in Table II. While its average lead times decrease by 0.17s and 0.09s for non-angled and angled critical faults, respectively, the corresponding average false positive rates also rise to 0.08 for both cases. This indicates a decline in the nominal critical fault classifier’s performance. This decline in performance is particularly apparent for side pushes, as the false positive rates for critical faults applied to the sides of the robot are on average 0.13 for both angled and non-angled critical faults, whereas for torso-based critical faults, the rates are 0.02 and 0.04 for non-angled and angled forces, respectively. These results align with expectations, as the model’s training data primarily focuses on faults introduced along the sagittal plane and does not adequately capture the variability of side or angled faults.

Metrics	Nominal			Fine-Tuned		
	Non Ang	Ang.	In Dist	Non Ang	Ang	In Dist
FPR	0.08	0.08	0.0	0.0	0.003	0.0
Lead Time	1.35	1.43	1.52	1.18	1.26	1.18
Response Time	0.42	0.41	0.44	0.59	0.59	0.62

TABLE II: Nominal [1] and Fine-Tuned Critical Fault Classifier results evaluated on non-angled and angled abrupt and incipient faults introduced by forces applied at various locations on the robot. **Acronyms used:** Non ang (non-angled), ang (angled), and in dist (in-distribution or tests from [1]).

C. Nominal Lead time classifier

When evaluated on in-distribution critical faults, the lead time classifier achieved accuracies of 1.0, 0.95, and 0.74 for the $[0, 1]$, $(1, 2]$, and $(2, H]$ lead time intervals, respectively [1]. However, similar to the critical fault classifier, the lead time classifier performs worse when evaluated on a broader range of critical faults. For non-angled critical faults,

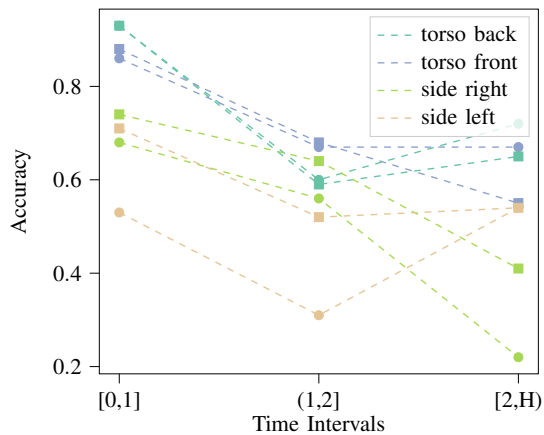


Fig. 6: Lead time classifier accuracies when evaluated on non-angled and angled critical faults across various locations. The circles and squares indicate the non-angled and angled critical faults, respectively.

the classifier, as shown in Table III, achieves accuracies of 0.82, 0.57, and 0.61 for the $[0,1]$, $(1,2]$, and $(2,H]$ intervals, respectively. For angled critical faults, the classifier achieves accuracies of 0.84, 0.63, and 0.55 for the same intervals. This decline in performance, as shown in Figure 6, is particularly pronounced for side critical faults. These results mirror those of the critical fault classifier and are consistent with expectations, given that the training data consists solely of faults introduced along the sagittal plane. Furthermore, the lead time classifier achieves its highest accuracy within the $[0,1]$ interval, which is consistent with the findings in [1], where it is noted that the number of data points decreases exponentially as lead time increases. The asymmetry observed in Figure 6 between the left and right sides can be attributed to randomness in data generation, leading to varying force magnitudes even within the same range. When critical faults from one side are emulated on the other, the lead time classifier produces similar results.

Intervals	Nominal			Fine-Tuned		
	Non Ang	Ang	In Dist	Non Ang	Ang	In Dist
$[0,1]$	0.82	0.84	1.0	0.96	0.95	0.98
$(1,2]$	0.57	0.63	0.95	0.84	0.80	0.82
$[2,H]$	0.61	0.55	0.74	0.30	0.27	0.44

TABLE III: Nominal [1] and Fine-Tuned Lead Time Classifier results evaluated on non-angled and angled abrupt and incipient faults introduced by forces applied at various locations on the robot. **Acronyms used:** Non ang (non-angled), ang (angled), and in dist (in-distribution or tests from [1]).

D. Nominal Lead time regressor

When evaluated on in-distribution critical faults within the $[0,1]$ lead time range, the lead time regressor shows minimal error, with a maximum difference of 0.09s between predicted and actual lead time, and a mean and median difference

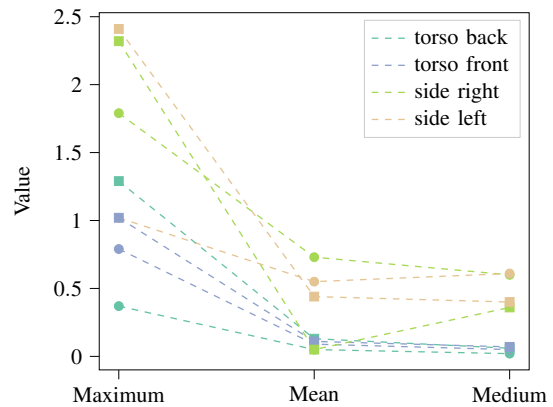


Fig. 7: Regressor results when evaluated on non-angled and angled critical faults across various locations. The circles and squares indicate the non-angled and angled critical faults, respectively.

of just 0.01s [1]. However, similar to both the critical fault classifier and the lead time classifier, the regressor performs significantly worse on non-angled and angled critical faults. For non-angled critical faults, the maximum lead time prediction error increases to 1.79s, while the mean and median errors rise to 0.23s and 0.07s, respectively, as shown in Table IV. For critical angled faults, the maximum error increases to 2.41s, with mean and median errors of 0.25s and 0.11s, respectively. Given that the regressor's objective is to predict lead time within the $[0,1]$ interval, these error increases are unacceptable. Despite these significant errors, as shown in Figure 7, the regressor performs better for the torso back non-angled critical faults compared to the other regions and faults.

Differences	Nominal			Fine-Tuned		
	Non Ang	Ang	In Dist	Non Ang	Ang	In Dist
Max	1.79	2.41	0.09	0.23	0.32	0.18
Mean	0.23	0.25	0.01	0.03	0.03	0.04
Median	0.07	0.11	0.01	0.02	0.02	0.03

TABLE IV: Nominal and Fine-Tuned Lead Time Regressor results evaluated on non-angled and angled abrupt and incipient faults introduced by forces applied at various locations on the robot. **Acronyms used:** Non ang (non-angled), ang (angled), and in dist (in-distribution or tests from [1]).

V. FINE-TUNING THE NOMINAL FALL PREDICTION ALGORITHM

This section explores strategies to enhance the robustness of the nominal fall prediction algorithm against omnidirectional faults, addressing its suboptimal performance, particularly when faults are introduced by forces applied to the frontal plane. A common challenge with learning-based methods is their reliance on large datasets. To mitigate this while leveraging the existing algorithm, we focus on fine-tuning the existing critical fault classifier, lead time classifier, and lead time regressor. Our goal is to improve performance

while minimizing the need for additional training data, thus striking a balance between performance and data efficiency.

Fine-tuning is a widely used machine learning technique that adapts a pre-trained model to new data by leveraging previously learned features while adjusting to the specific requirements of the new task. This approach is both efficient and effective, especially when the new data closely resembles the original data used for pre-training. Compared to training a model from scratch, fine-tuning enables rapid adaptation to new tasks with significantly less computational effort [33].

For our task of standing, it is reasonable to assume that detecting faults from omnidirectional pushes shares enough similarity with the nominal algorithm's training scenario, which involves detecting faults from pushes applied to the center-back of the robot's torso. In fact, when we compared the performance of the fine-tuned model to that of a model trained from scratch, we found their performance to be comparable.

A. Fine-Tuned Critical Fault Classifier Results

Given the nominal critical fault classifier's poor performance on unsafe side trajectories, as discussed in Section IV-B, it is fine-tuned with 200 non-angled abrupt and 200 non-angled incipient faults, each applied to region B of side left and right, as shown in Figure 5. These regions are selected because they represent the "midpoint" of the possible pushing areas on the sides.

Compared to the nominal critical fault classifier, the average false positive rates for the fine-tuned critical fault classifier, as shown in Table II, decreases significantly—from 0.08 to 0.0 for non-angled faults, and from 0.08 to 0.003 for angled faults. As expected, due to the direct relationship between false positive rate and lead time, the average lead time decreases from 2.54s to 1.18s and from 2.41s to 1.26s for non-angled and angled critical faults, respectively. On the other hand, the average response time increases by 0.16s and 0.17s, respectively, for non-angled and angled critical faults.

When evaluated on in-distribution data, the fine-tuned model achieves a 0.0 average false positive rate, similar to the nominal model. However, the average lead time and response time decrease and increase by 0.34s and 0.18s, respectively. Despite this, the fine-tuned critical fault classifier model achieves lead times significantly above 0.2s and nearly 0 false positive rates for all critical faults, meeting the objective outlined in [1] of detecting critical faults with sufficient lead time.

B. Fine-Tuned Lead Time Classifier Results

The lead time classifier is fine-tuned using data from the same regions as the critical fault classifier. After fine-tuning, the lead time classifier's accuracy, as shown in Table III, increases from 0.82 to 0.96 and from 0.84 to 0.95 for the non-angled and angled critical faults in the $[0, 1]$ interval, respectively. The accuracy also increases from 0.57 to 0.84 and from 0.63 to 0.80 for the $(1, 2]$ interval. However, the accuracy decreases from 0.61 to 0.30 and from 0.55 to 0.27, respectively, for the $(2, H]$. This decline is expected and

acceptable given that the number of data points decreases exponentially as lead time increases [1].

When evaluated on in-distribution data, the fine-tuned model's performance slightly decreases. The accuracies drop by 0.02, 0.13, and 0.3 for the $[0, 1]$, $(1, 2]$, and $(2, H]$ intervals, respectively. While the drop in performance for the $(2, H]$ interval might seem significant, it is justifiable due to the previously mentioned exponential relationship between lead time and data availability. Furthermore, given the long lead times in this interval, exceeding the 0.2s threshold [1], it is reasonable to disregard the classifier's output for this region, as it will not have severe consequences before transitioning to intervals with more accurate predictions.

C. Fine-Tuned Lead Time Regressor Results

Fine-tuning the lead time regressor using the same data as the critical fault and lead time classifier results in only acceptable performance for non-angled critical faults. Therefore, the lead time regressor is instead fine-tuned with 200 angled abrupt faults and 200 angled incipient faults, applied to the following regions: side left B and C, side right B and C, and torso front C. When evaluated on the in-distribution data, the maximum, mean, and median differences, as shown in Table IV, increase by 0.09s, 0.03s, and 0.02s, respectively, compared to the nominal model. However, when assessed on non-angled critical faults, the maximum, mean, and median differences decrease from 1.79s to 0.23s, from 0.23s to 0.03s, and from 0.07s to 0.02s, respectively, for non-angled critical faults. Similarly, for angled critical faults, the differences decrease from 2.41s to 0.32s, from 0.25s to 0.03s, and from 0.08s to 0.02s. Despite the substantial improvement in maximum difference for both angled and non-angled critical faults, the maximum difference of 0.32s achieved for angled critical faults may appear significant within the $[0, 1]$ interval; however, the classifier attains this maximum difference in only 1 percent of the unsafe trajectories. This, along with the notable decrease in maximum difference, underscores the lead time regressor fine-tuned model's capability to perform well across a wide range of critical faults.

VI. CONCLUSION

In this paper, we extended the nominal fall prediction algorithm from [1] to a real-time setting, implementing it in both hardware and simulation. The online implementation yields results similar to the offline version when tested on comparable data. Additionally, in simulation, it achieves an average recovery rate of 0.97. The average runtime in simulation and hardware is approximately 0.0045s and 0.0061s, respectively. The difference of 0.0061s is deemed negligible given the algorithm's sampling rate of 0.025s (40Hz). Given the similar results between offline simulation and hardware implementations shown in [1], along with the consistent performance between online and offline simulations and between online and offline hardware implementations, and the comparable runtimes between online hardware and simulation implementations, we conclude that offline simulation

results are reliable indicators of online performance, and simulation results can effectively predict hardware outcomes.

To further assess the algorithm’s robustness, we evaluated the nominal fall prediction algorithm against a broader range of faults. This evaluation is performed for each of the three components: the critical fault classifier, the lead time classifier, and the lead time regressor. When assessed on this broader range of faults, all three components performed significantly worse—especially for faults in the frontal plane—compared to the results in [1].

To improve the nominal fall prediction algorithm’s performance on this broader fault set while minimizing the need for additional data, we fine-tuned the three components with additional data. The fine-tuned components significantly outperformed the nominal components across all evaluation metrics. Furthermore, the fine-tuned algorithm achieved an average lead time greater than 0.2s with nearly 0 average false positive rate, and a maximum average mean difference of 0.03s for the lead time. These results highlight the fine-tuned fall prediction algorithm’s suitability for real-time and offline fall and lead time prediction in bipedal robots, even across a wide variety of faults.

REFERENCES

- [1] M. E. Mungai, G. Prabhakaran, and J. W. Grizzle, “Fall prediction for bipedal robots: The standing phase,” in *2024 IEEE International Conference on Robotics and Automation (ICRA)*. IEEE, 2024, pp. 13 135–13 141.
- [2] BMW Group, “Successful test of humanoid robots at bmw group plant spartanburg,” <https://www.press.bmwgroup.com/global/article/detail/T0444265EN/successful-test-of-humanoid-robots-at-bmw-group-plant-spartanburg?language=en>, 2024, accessed: 11.16.2024.
- [3] Tech Crunch, “Figure will start ‘alpha testing’ its humanoid robot in the home in 2025,” <https://techcrunch.com/2025/02/27/figure-will-start-alpha-testing-its-humanoid-robot-in-the-home-in-2025/>, 2025, accessed: 19.04.2025.
- [4] Boston Dynamics, “An electric new era for atlas,” <https://bostondynamics.com/blog/electric-new-era-for-atlas/>, 2024, accessed: 11.16.2024.
- [5] Aptronik and Mercedes-Benz, “Aptronik and mercedes-benz enter commercial agreement,” <https://aptronik.com/news-collection/aptronik-and-mercedes-benz-enter-commercial-agreement>, 2024, accessed: 11.16.2024.
- [6] GXO and Aptronik, “Gxo advances humanoid strategy with aptronik,” <https://aptronik.com/news-collection/gxo-advances-humanoid-strategy-with-aptronik>, 2024, accessed: 11.16.2024.
- [7] Agility Robotics, “Agility robotics announces strategic investment and agreement with motion technology company schaeffler group,” <https://agilityrobotics.com/content/agility-robotics-announces-strategic-investment-and-agreement-with-protectpenalty-\@M-motiontechnology-company-schaeffler-group>, accessed: 11.16.2024.
- [8] C. Yu, “Humanoids make waves on factory floors,” <https://www.chinadaily.com.cn/a/202410/17/WS67107018a310f1265a1c811f.html>, 2024, accessed: 11.16.2024.
- [9] Sanctuary AI, “A transformational few months for sanctuary ai,” <https://www.sanctuary.ai/blog/a-transformational-few-months-for-sanctuary-ai>, 2024, accessed: 11.16.2024.
- [10] L. Kolodny and A. Levy, “Elon musk claims optimus robots could make tesla a \$25 trillion company – more than half the value of the s&p 500 today,” <https://www.cnbc.com/2024/06/13/elon-musk-says-optimus-robots-could-make-tesla-25-trillion-company-.html>, 2024, accessed: 11.16.2024.
- [11] 1x, “Introducing neo gamma,” <https://www.1x.tech/discover/introducing-neo-gamma>, 2025, accessed: 19.04.2025.
- [12] M. E. Mungai and J. Grizzle, “Optimizing lead time in fall detection for a planar bipedal robot,” in *2023 3rd International Conference on Electrical, Computer, Communications and Mechatronics Engineering (ICECCME)*, 2023, pp. 1–7.
- [13] R. Isermann, “Process fault detection based on modeling and estimation methods,” *IFAC Proceedings Volumes*, vol. 15, no. 4, pp. 7–30, 1982, 6th IFAC Symposium on Identification and System Parameter Estimation, Washington USA, 7-11 June. [Online]. Available: <https://www.sciencedirect.com/science/article/pii/S1474667017629598>
- [14] R. Subburaman, D. Kanoulas, N. Tsagarakis, and J. Lee, “A survey on control of humanoid fall over,” *Robotics and Autonomous Systems*, vol. 166, p. 104443, 2023.
- [15] B. Zhang and M. Jia, “Fall recovery strategies in humanoid robots: A brief survey,” in *2023 8th International Conference on Control, Robotics and Cybernetics (CRC)*. IEEE, 2024, pp. 68–72.
- [16] R. Subburaman, D. Kanoulas, L. Muratore, N. G. Tsagarakis, and J. Lee, “Human inspired fall prediction method for humanoid robots,” *Robotics and Autonomous Systems*, vol. 121, p. 103257, 2019.
- [17] N. G. Tsagarakis, D. G. Caldwell, F. Negrello, W. Choi, L. Baccelliere, V.-G. Loc, J. Noorden, L. Muratore, A. Margan, A. Cardellino, *et al.*, “Walk-man: A high-performance humanoid platform for realistic environments,” *Journal of Field Robotics*, vol. 34, no. 7, pp. 1225–1259, 2017.
- [18] T. Wu, Z. Yu, X. Chen, C. Dong, Z. Gao, and Q. Huang, “Falling prediction based on machine learning for biped robots,” *Journal of Intelligent & Robotic Systems*, vol. 103, pp. 1–14, 2021.
- [19] J. Igual, P. Parik-Americano, E. C. Becman, and A. Forner-Cordero, “Time series classification for predicting biped robot step viability,” *Sensors*, vol. 24, no. 22, p. 7107, 2024.
- [20] D. H. Tran, F. Hamker, and J. Nassour, “A humanoid robot learns to recover perturbation during swinging motion,” *IEEE Transactions on Systems, Man, and Cybernetics: Systems*, vol. 50, no. 10, pp. 3701–3712, 2020.
- [21] K. Saleh, T. O’Brien, Y. Sims, A. Mendes, and S. Chalup, “Efficient sequence model for early fall detection of humanoid robots,” in *RoboCup 2024: Robot World Cup XXVII*, E. Barros, J. P. Hanna, H. Okada, and E. Torta, Eds. Cham: Springer Nature Switzerland, 2025, pp. 247–256.
- [22] C. Zhang, J. Gao, Z. Chen, S. Zhong, and H. Qiao, “Fall analysis and prediction for humanoids,” *Robotics and Autonomous Systems*, vol. 190, p. 104995, 2025. [Online]. Available: <https://www.sciencedirect.com/science/article/pii/S0921889025000818>
- [23] C. Chevallereau, G. Abba, Y. Aoustin, F. Plestan, E. Westervelt, C. C. De Wit, and J. Grizzle, “Rabbit: A testbed for advanced control theory,” *IEEE Control Systems Magazine*, vol. 23, no. 5, pp. 57–79, 2003.
- [24] Y. Gong, R. Hartley, X. Da, A. Hereid, O. Harib, J.-K. Huang, and J. Grizzle, “Feedback control of a cassie bipedal robot: Walking, standing, and riding a segway,” in *2019 American control conference (ACC)*. IEEE, 2019, pp. 4559–4566.
- [25] Aldebaran, “Nao,” <https://corporate-internal-prod.aldebaran.com/en/nao>, accessed: 11.16.2024.
- [26] —, “H25 - construction,” http://doc.aldebaran.com/2-1/family/nao_h25/dimensions_h25.html, accessed: 11.16.2024.
- [27] Agility Robotics, “Robots,” <https://agilityrobotics.com/products>.
- [28] M. E. Mungai, G. Prabhakaran, and J. W. Grizzle, “Digit fall prediction dataset,” https://github.com/UMich-BipedLab/Digit_Fall_Prediction_Dataset, 2023.
- [29] H. Safaeipour, M. Forouzanfar, and A. Casavola, “A survey and classification of incipient fault diagnosis approaches,” *Journal of Process Control*, vol. 97, pp. 1–16, 2021. [Online]. Available: <https://www.sciencedirect.com/science/article/pii/S0959152420303206>
- [30] G. Gibson, “Terrain-aware bipedal locomotion,” Ph.D. dissertation, University of Michigan, 2023.
- [31] M. Quigley, K. Conley, B. Gerkey, J. Faust, T. Foote, J. Leibs, R. Wheeler, A. Y. Ng, *et al.*, “Ros: an open-source robot operating system,” in *ICRA workshop on open source software*, vol. 3, no. 3.2. Kobe, Japan, 2009, p. 5.
- [32] D. Hendrycks and K. Gimpel, “A baseline for detecting misclassified and out-of-distribution examples in neural networks,” *CoRR*, vol. abs/1610.02136, 2016. [Online]. Available: <http://arxiv.org/abs/1610.02136>
- [33] J. Howard and S. Ruder, “Universal language model fine-tuning for text classification,” 2018. [Online]. Available: <https://arxiv.org/abs/1801.06146>